



Published in final edited form as:

Nature. 2013 June 6; 498(7452): 118–122. doi:10.1038/nature12166.

## Control of Angiogenesis by AIBP-mediated Cholesterol Efflux

Longhou Fang<sup>1</sup>, Soo-Ho Choi<sup>1</sup>, Ji Sun Baek<sup>1</sup>, Chao Liu<sup>1</sup>, Felicidad Almazan<sup>1</sup>, Florian Ulrich<sup>2</sup>, Philipp Wiesner<sup>1</sup>, Adam Taleb<sup>1</sup>, Elena Deer<sup>1</sup>, Jennifer Pattison<sup>1</sup>, Jesús Torres-Vázquez<sup>2</sup>, Andrew C. Li<sup>1,#</sup>, and Yury I. Miller<sup>1,\*</sup>

<sup>1</sup>Department of Medicine, University of California, San Diego, 9500 Gilman Drive, La Jolla, CA 92093

<sup>2</sup>Helen L. and Martin S. Kimmel Center for Biology and Medicine, Skirball Institute of Biomolecular Medicine, New York University Langone Medical Center, 540 First Avenue, New York, NY 10016

### Abstract

Cholesterol is a structural component of the cell, indispensable for normal cellular function, but its excess often leads to abnormal proliferation, migration, inflammatory responses and/or cell death. To prevent cholesterol overload, ATP-binding cassette (ABC) transporters mediate cholesterol efflux from the cells to apolipoprotein A-I (ApoA-I) and to the ApoA-I-containing high-density lipoprotein (HDL)<sup>1-3</sup>. Maintaining efficient cholesterol efflux is essential for normal cellular function<sup>4-6</sup>. However, the role of cholesterol efflux in angiogenesis and the identity of its local regulators are poorly understood. Here we show that ApoA-I binding protein (AIBP) accelerates cholesterol efflux from endothelial cells (EC) to HDL and thereby regulates angiogenesis. AIBP/HDL-mediated cholesterol depletion reduces lipid rafts, interferes with VEGFR2 dimerization and signaling, and inhibits VEGF-induced angiogenesis *in vitro* and mouse aortic neovascularization *ex vivo*. Remarkably, Aibp regulates the membrane lipid order in embryonic zebrafish vasculature and functions as a non-cell autonomous regulator of zebrafish angiogenesis. Aibp knockdown results in dysregulated sprouting/branching angiogenesis, while forced Aibp expression inhibits angiogenesis. Dysregulated angiogenesis is phenocopied in Abca1/Abcg1-deficient embryos, and cholesterol levels are increased in Aibp-deficient and Abca1/Abcg1-deficient embryos. Our findings demonstrate that secreted AIBP positively regulates cholesterol efflux from EC and that effective cholesterol efflux is critical for proper angiogenesis.

---

Users may view, print, copy, download and text and data-mine the content in such documents, for the purposes of academic research, subject always to the full Conditions of use: [http://www.nature.com/authors/editorial\\_policies/license.html#terms](http://www.nature.com/authors/editorial_policies/license.html#terms)

\*Corresponding author: Yury I. Miller, Department of Medicine, University of California, San Diego, 9500 Gilman Drive, La Jolla, CA 92093. Tel: 858-822-5771. [yumiller@ucsd.edu](mailto:yumiller@ucsd.edu).

#Deceased

The authors declare no conflicts of interests.

**Author Contributions:** F.L. and Y.I.M. conceived the project, designed the experiments and wrote the manuscript. J.T.-V. made important intellectual contributions and helped revise the manuscript. F.L. performed the majority of the experiments. S.H.C., J.S.B., C.L., F.A., F.U., P.W., A.T., E.D., J.P., A.C.L. performed experiments and/or provided research assistance.

**Author Information:** Reprints and permissions information is available at [www.nature.com/reprints](http://www.nature.com/reprints). The authors declare no competing financial interests.

AIBP is a secreted protein discovered in a screen of proteins that physically associate with ApoA-I<sup>7</sup>. Human *APOAIBP* mRNA encoding the AIBP protein is ubiquitously expressed<sup>7</sup>. Although the AIBP binding to ApoA-I implies that AIBP may modulate HDL function<sup>7,8</sup>, its role in cholesterol efflux has not been experimentally tested.

First, we investigated whether human AIBP (hAIBP) had any effect on cholesterol removal from human umbilical vein endothelial cells (HUVEC) in which ABCG1 is a major transporter responsible for cholesterol efflux to HDL<sup>9,10</sup>. In the presence of hAIBP, cholesterol efflux from HUVEC to HDL<sub>3</sub> was increased 2-fold, and the ABCG1 deficiency completely abrogated this effect (Fig. 1a, Supplementary Fig. 2). hAIBP did not promote cholesterol efflux in absence of HDL<sub>3</sub> (Supplementary Fig. 2b), but the hAIBP binding to HUVEC (Supplementary Fig. 3) increased the overall HUVEC capacity to bind HDL<sub>3</sub> ( $B_{\max}=1.5$  vs. 0.8) and the constant of HDL<sub>3</sub> dissociation from HUVEC ( $K_d=1.0\times 10^{-6}$ M vs.  $0.33\times 10^{-6}$ M; Figs. 1b, c), thereby creating conditions that would facilitate HDL<sub>3</sub>-mediated cholesterol efflux.

To investigate the role of AIBP/HDL-mediated cholesterol efflux in angiogenesis, we incubated HUVEC with hAIBP and/or HDL<sub>3</sub> and then stimulated cells with VEGF. hAIBP and HDL<sub>3</sub> added separately did not affect EC tube formation, but together they significantly reduced angiogenesis (Fig. 1d, e and Supplementary Fig. 4). Cholesterol depletion by methyl- $\beta$ -cyclodextrin (M $\beta$ CD)<sup>11</sup> also inhibited angiogenesis, whereas cholesterol-loaded M $\beta$ CD, which delivers cholesterol to the cell, promoted angiogenesis (Supplementary Fig. 5). If the hAIBP/HDL<sub>3</sub> inhibition of angiogenesis is the consequence of accelerated cholesterol efflux, then this effect should depend on the presence of the cholesterol transporter ABCG1. Indeed, knockdown of ABCG1 in HUVEC rescued VEGF-induced angiogenesis from the hAIBP/HDL<sub>3</sub> inhibition (Fig. 1f). Further, we tested both hAIBP and zAibp2 (a zebrafish protein, which will be discussed later) in an *ex vivo* aortic ring angiogenesis assay. A cluster of HEK293 cells producing either hAIBP, zAibp2 or mCherry (negative control) was placed 0.5 mm from the edge of a mouse aortic ring, and VEGF was added to stimulate angiogenesis. Both hAIBP and zAibp2, but not mCherry, significantly reduced neovascularization of aortic rings isolated from a wild type mouse (Figs. 1g, h). Aortic rings from an *Abcg1*<sup>-/-</sup> mouse responded to VEGF with a more vigorous angiogenesis, which was not significantly reduced by hAIBP or zAibp2. These results support the hypothesis that cholesterol efflux is necessary for the AIBP-mediated inhibition of angiogenesis.

HDL-mediated depletion of cholesterol from plasma membrane disrupts cholesterol- and sphingomyelin-rich membrane microdomains<sup>12,13</sup>, often designated as lipid rafts, and affects membrane receptor signaling<sup>11</sup>. We found that hAIBP/HDL<sub>3</sub> reduced the lipid raft content in HUVEC and disrupted cell-surface colocalization of caveolin-1 and VEGFR2 (Figs. 2a-c and Supplementary Fig. 6). The hAIBP/HDL<sub>3</sub> treatment, similarly to the treatment with M $\beta$ CD, decreased VEGFR2 and caveolin-1 localization to the lipid raft fraction isolated from cell lysates (Fig. 2d and Supplementary Fig. 7). Many studies suggest that VEGFR2 localization to lipid rafts facilitates VEGFR2 dimerization and endocytosis<sup>14-17</sup>, the steps required for VEGF-mediated signaling<sup>18</sup>. In our experiments, the hAIBP/HDL<sub>3</sub> treatment reduced VEGF-induced VEGFR2 dimerization and endocytosis as

well as phosphorylation of VEGFR2, Akt, FAK, Src and to a lesser degree of ERK1/2 (Figs. 2e-g and Supplementary Figs. 8-10). Importantly, subsequent addition of cholesterol partially reversed inhibition of VEGFR2, FAK and Akt phosphorylation in hAIBP/HDL<sub>3</sub>-treated cells (Supplementary Fig. 11). Consistent with the effect on VEGF signaling, HUVEC migration toward a VEGF cue was significantly reduced in hAIBP/HDL<sub>3</sub>-treated cells (Supplementary Fig. 12). These results suggest that hAIBP facilitates cholesterol efflux from HUVEC to HDL and that cholesterol depletion of the plasma membrane disrupts lipid rafts and VEGF signaling and inhibits VEGF-induced angiogenesis.

AIBP is evolutionary conserved from *Drosophila* to zebrafish to mouse and human (Supplementary Fig. 13a). Zebrafish have two genes, *apoalbp1* and *apoalbp2*, encoding zAibp1 and zAibp2 proteins, respectively (Supplementary Fig. 13b). The *zaiBP2* expression in 24-36 hours postfertilization (hpf) zebrafish embryos shows a clear segmental pattern, colocalizing with the somite marker *myod* (Fig. 3a and Supplementary Fig. 14). By 48 hpf, when segmental angiogenesis is completed, *zaiBP2* is no longer expressed in somites.

Both zAibp2 and zAibp1 bound to human ApoA-I and to the HDL in human plasma, but only zAibp2 was effective in promoting cholesterol efflux from HUVEC to HDL<sub>3</sub> (Supplementary Figs. 15, 16). Zebrafish embryos injected with antisense morpholino oligonucleotides (MO) targeting *zaiBP2* translation sites had increased levels of free (unesterified) cholesterol, whereas injections of *zaiBP1* or scrambled control MO did not result in any changes (Figs. 3b, c and Supplementary Fig. 17). Thus, we focused on *zaiBP2*. Using the polarity-sensitive fluorescent probe Laurdan, we observed a higher membrane lipid order in the areas of growing segmental arteries (SeA) corresponding to tip cells compared to stalk cells (Fig. 3d, e), suggesting a higher content of lipid rafts in tip cells, which may positively regulate Vegfr2 signaling. The membrane lipid order was increased in the SeA of *zaiBP2* morphants compared to controls, and the difference between tip and stalk cells was lost. To test the hypothesis that zAibp2-mediated cholesterol efflux regulates membrane order in growing SeA, we injected *zaiBP2* morphants with human HDL<sub>3</sub> or with BSA. Adding an excess of HDL<sub>3</sub> – to promote cholesterol efflux and to override the zAibp2 deficiency – annulled the increase in membrane order in SeA of *zaiBP2* morphants, and a spatially indiscriminate HDL<sub>3</sub> excess equalized the membrane order in tip and stalk cells. Adding an excess of BSA had no effect on the membrane order in *zaiBP2* morphants. Lysates of *zaiBP2* knockdown embryos displayed increased phosphorylation of Vegfr2, Akt and Src, and decreased phosphorylation of Erk1 (Fig. 3f, Supplementary Figs. 18, 19). These results suggest that zAibp2 regulates cholesterol levels, the membrane lipid order, and Vegfr2 signaling and, thus, may control angiogenesis.

Indeed, injection of MOs targeting *zaiBP2* translation or splicing sites into one-cell stage embryos of *Tg(fli1:egfp)<sup>y1</sup>* zebrafish, which express EGFP in EC<sup>19</sup>, resulted in remarkable dysregulation of angiogenesis, with profound ectopic branching of both SeA and subintestinal veins (SIV) (Fig. 3g and Supplementary Figs. 20, 21). The *zaiBP2* knockdown was validated in western blot (Fig. 3f). The ectopic branching of SeAs in *zaiBP2* morphants was partially rescued by forced expression of *zaiBP2* mRNA lacking the MO target site (Fig. 3h).

The *zaiBP2* expression pattern (Fig. 3a) resembles that of type 3 semaphorins, non-cell autonomous repellent cues that guide the patterning of developing SeAs via endothelial-specific PlexinD1 receptors<sup>20</sup>. To determine the cell autonomy of the zAibp2 effect on angiogenesis, we performed cell transplantation experiments, using *Tg(fli1:egfp)<sup>y1</sup>* donors. Fluorescent EC from wild type donors found in non-fluorescent *zaiBP2* morphants displayed excessive branching and filopodial projections, while fluorescent EC from *zaiBP2* morphant donors found in wild type recipients had normal morphology (Figs. 4a, b). In a gain-of-function experiment, overexpression of zAibp2 inhibited SeA sprouting from the dorsal aorta and normal growth of sprouted SeA (Supplementary Fig. 22). These results suggest a role for zAibp2 as a repellent molecule whose function depends on the milieu surrounding EC but not on zAibp2 expression in the EC themselves.

The loss of zAibp2 resulted in increased expression of genes involved in angiogenesis, such as *tie2*, *vegfr2*, *vegfr3* and *fli1* (Supplementary Figs. 23-24). Thus, in addition to the zAibp2 effect on the membrane lipid order and Vegfr2 signaling (Figs. 3d-f), zAibp2 affects expression of angiogenic genes as well.

To further validate that effective cholesterol efflux is required for normal angiogenesis, we knocked down zebrafish cholesterol transporters *abca1* and *abcg1*<sup>21,22</sup> and observed higher levels of free cholesterol, increased levels of phosphorylated Akt, Vegfr2 and Src and dysregulated SeA and SIV angiogenesis (Figs. 3f, 4c and Supplementary Figs. 19, 25-27), closely reproducing the angiogenesis defects of *zaiBP2* morphants. Individual knockdown of each *abca1* and *abcg1* suggested a dominant role of *abca1* in embryonic angiogenesis (Supplementary Fig. 28). In contrast to the *zaiBP2* non-cell autonomous regulation of angiogenesis, fluorescent EC from *abca1/abcg1* morphant donors found in wild type recipients displayed excessive SeA branching (Figs. 4a, b), confirming that cholesterol efflux from EC is required to restrain ectopic angiogenesis. Overexpression of zAibp2-mCherry in somites resulted in inhibition of SeA growth, which was rescued by knocking down *abca1/abcg1* (Figs. 4d, e). These results provide additional evidence that expression of zAibp2 limits blood vessel growth and also suggest that zebrafish Abca1- and/or Abcg1-mediated cholesterol efflux is required for the zAibp2 effect on angiogenesis.

Based on our results, we propose that there is an additional level of paracrine regulation of the VEGFR2 pathway in which cholesterol efflux and associated reduction of ordered membrane microdomains/lipid rafts interfere with the VEGFR2 membrane localization, dimerization, endocytosis, and signaling. Because in 24 hpf zebrafish *zaiBP2* mRNA is highly expressed in somites, but not in the inter-somitic spaces where SeA grow, it is likely that zAibp2-mediated cholesterol efflux inhibits Vegfr2 signaling in a site-specific manner to prevent lateral protrusions from stalk and tip cells and restrains ectopic SeA growth into somites (Supplementary Fig. 1).

The role of cholesterol efflux mechanisms in protecting against endothelial dysfunction, in particular in hypercholesterolemic animals prone to development of atherosclerosis, has been reported<sup>10,23</sup>. However, our study is the first to demonstrate the role of AIBP in promoting cholesterol efflux from EC to HDL and the importance of this mechanism in regulation of angiogenesis. In contrast to the ApoA-I-containing HDL, ApoB-containing

LDL and VLDL deliver cholesterol and other lipids to the cell and, thus, are positioned to promote angiogenesis. Interestingly, a recent paper finds the opposite, that ApoB lipoproteins negatively regulate angiogenesis in zebrafish embryos<sup>24</sup>. The authors suggest a mechanism in which the ApoB protein, but not the lipid components within ApoB-containing lipoproteins, is responsible for transcriptional regulation of Vegfr1, a soluble decoy receptor for Vegf. Our experiments uncovered a different, lipid-mediated mechanism in which effective cholesterol efflux is a critical process that ensures proper angiogenesis and Aibp secreted by the surrounding tissues serves as an important negative regulator of angiogenesis.

## Full Methods

### Cloning of human and zebrafish AIBP, recombinant protein expression and purification, and antibody production

Zebrafish *aibp2* (Gene ID:557840) and *aibp1* (Gene ID:436891) were cloned from zebrafish brain cDNA using primers: CCGGAATTCCATGTTGGGGGTTTCGAGCTCTG (5') and CGCGGATCCTCAGTTGAGCTGAAACACACTC (3') for *zaiBP1*; and CCGGAATTCCGCCACCATGAACCACAGCTCCAACG (5') and CGCGGATCCCAGCTTCTATAATACATTCTGTGC (3') for *zaiBP2*. The fragments were cloned in frame into pFLAG-CMV4 (Sigma). Human *APOA1BP* (Gene ID: 128240) was cloned from HEK293 cell cDNA using primers: CCGGAATTCCATGTCCAGGCTGCGGGCGCTGCTGGGCCTCG (5') and CGGGGTACCTCACTGCAGACGATAGACACTC (3'). For expression of AIBP proteins, the genes were cloned in frame into pHUE vector<sup>26</sup> (kindly provided by Tracy Handel), expressed in BL21 DE3 competent cells (Invitrogen) and purified with a Ni-NTA agarose resin column (Qiagen). Deubiquitinase (DUB) expressed in pHUE was used as a negative control in experiments with recombinant AIBP. To produce a zAibp2 antibody, recombinant zAibp2 was mixed with complete Freund's adjuvant (Sigma) and injected subcutaneously into a guinea pig. The guinea pig was boosted 3 more times. Post-immune plasma was compared with pre-immune plasma from the same animal and used in western blot to detect zAibp2 in zebrafish lysates (Supplementary Fig. 18). The specificity of the antibody was confirmed by adding excess of recombinant zAibp2 to the antibody, which prevented its binding to a specific band on the western blot.

### Cholesterol efflux

A cholesterol efflux assay was performed as described<sup>23,27</sup>, with modifications. In brief, HUVEC (ATCC) were loaded with 2  $\mu\text{Ci/ml}$  <sup>3</sup>H-cholesterol, and cholesterol efflux was initiated by the addition of 0.2% BSA/EBM with 50  $\mu\text{g/ml}$  HDL<sub>3</sub> (isolated from normolipidemic human plasma by ultracentrifugation), in the presence or absence of 0.2  $\mu\text{g/ml}$  zAibp2, zAibp1, or hAIBP. DUB, replacing AIBP, was used as a negative control. Background, non-specific release of <sup>3</sup>H-cholesterol was measured in absence of HDL or any other protein. After 1 to 6 hours of incubation, the medium was collected and counted in a liquid scintillation counter LS 6500 (Beckman Coulter). The cells were extracted with 2-propanol, and the lipid extract was added to ScintiVerse BD Cocktail (Fisher) and counted. Cholesterol efflux was expressed as a percentage of <sup>3</sup>H counts in the medium compared to

combined  $^3\text{H}$  counts in the cells and the medium. Background, non-specific release of  $^3\text{H}$  from the cells was subtracted.

### ABCG1 knockdown

Both negative control and *ABCG1* siRNA oligonucleotides were from Ambion. HUVEC were plated in 6-well plates at  $5 \times 10^5$  cells/well and transfected with 66.6 nM siRNA using SuperFect Transfection Reagent (Qiagen) as described in the manufacturer's protocol. Two days after transfection, cells were washed and used in an efflux assay. Two additional wells of transfected cells were used to confirm ABCG1 knockdown in western blot using an antibody from Novus Biologicals.

### AIBP/HDL<sub>3</sub> - HUVEC binding assay

hAIBP and HDL<sub>3</sub> were biotinylated with EZ-Link Sulfo-NHS-Biotin (Thermo Scientific) according to the manufacturer's protocol. Binding of biotinylated hAIBP or biotinylated HDL<sub>3</sub> to HUVEC was assessed by a chemiluminescent binding assay as described by Fang *et al.*<sup>28</sup>, with modifications. HUVEC ( $2 \times 10^4$ ) were seeded into 96-well flat bottom plates in 5% FBS-EBM. After 72 h, plates were blocked with ice-cold 1% BSA-PBS for 30 min on ice, incubated with ice-cold biotinylated proteins for 2 h on ice, washed, and fixed with ice-cold 4% paraformaldehyde (PFA) in PBS for 30 min. HUVEC-bound biotinylated hAIBP or HDL<sub>3</sub> were detected with NeutrAvidin-conjugated alkaline phosphatase (Pierce) and LumiPhos 530 (Lumigen, Southfield, MI), using a Dynex luminometer (Dynex Technologies). Data were recorded as relative light units counted per 100 ms. All samples were assayed in triplicates. The parameters of hAIBP and HDL<sub>3</sub> binding to HUVEC ( $B_{\max}$  and  $K_d$ ) were calculated using a total and non-specific binding algorithm within the GraphPad Prism 5.0 software package. The following model was used:  $\text{H} + \text{C} \leftrightarrow \text{HC}$ , where H is unbound HDL<sub>3</sub>, C is cells, and HC is HDL<sub>3</sub> bound to the cells. The equations used for calculating binding parameters were:

$$[\text{HC}]_{\text{specific}} = B_{\max} \times [\text{H}] / ([\text{H}] + K_d)$$

$$[\text{HC}]_{\text{nonspecific}} = \mathbf{a} + \mathbf{b} \times [\text{H}]$$

$$[\text{HC}]_{\text{total}} = [\text{HC}]_{\text{specific}} + [\text{HC}]_{\text{nonspecific}}$$

where **a** is background and **b** is the slope of the linear fit of nonspecific binding. Goodness of fit of non-linear regression was estimated using  $R^2$  and standard deviation of residuals ( $Sy.x$ ), expressed in the same units as [H] and  $B_{\max}$ . A molecular mass of 80 kDa was used for the HDL protein.

### **In vitro angiogenesis assay**

The angiogenesis assay was carried out as described in reference<sup>29</sup>. Growth factor reduced Matrigel (BD Biosciences) was thawed at 4°C overnight and diluted with an equal volume of serum-free EBM medium (Lonza). Each well of 96-well plates was coated with 50 µl diluted Matrigel and incubated at 37°C for 1 hour. HUVEC were serum-starved and then pre-incubated with HDL<sub>3</sub> and/or hAIBP. Cells were harvested and added to Matrigel-coated plates at 1×10<sup>4</sup> cells per well in EBM, in the presence or absence of 20 ng/ml VEGF (R&D Systems). Following a 12 hour incubation, tubular structures were imaged with a phase contrast microscope.

### **Free cholesterol measurements in HUVEC**

HUVEC cholesterol levels were measured in cellular lipid extracts using a colorimetric assay (BioVision) as described<sup>14</sup>.

### **Aortic ring neovascularization assay**

The method was adopted from reference<sup>30</sup>, with modifications. Thoracic aorta was isolated from a 6-week old male C57BL6 mouse or an age and gender matched *Abcg1*<sup>-/-</sup> mouse (kindly provided by Catherine Hedrick, La Jolla Institute for Allergy and Immunology), cleaned from surrounding fat and connective tissue and sliced into 1 mm long rings. The aortic rings were placed in wells of a 48-well plate containing solidified Matrigel and then covered with additional Matrigel. Small wells were made in Matrigel approximately 0.5 mm from aortic rings and 50 µl aliquots of Matrigel containing 1×10<sup>5</sup> HEK293 cells transfected with mCherry (negative control), zAIBP2 or hAIBP were placed in these wells. After 10 min, each well was filled with EBM medium supplemented with 10 ng/ml VEGF and the plates were incubated at 37°C for 6 days. Media were changed every two days. The rings were photographed in phase contrast using a Nikon Eclipse Ti microscope.

### **Visualization of lipid rafts with cholera toxin B**

HUVEC were plated on glass coverslips and preincubated with 50 µg/ml HDL<sub>3</sub>, 0.1 µg/ml hAIBP, or 50 µg/ml HDL<sub>3</sub> + 0.1 µg/ml hAIBP for 4 hours. Cells were washed once with medium before the addition of 1 µg/ml Alexa Fluor 594-labeled cholera toxin B (CTB, from Invitrogen). Cells were incubated for 15 min at 4°C, washed with PBS, and then incubated for 15 min at 4°C with an anti-CTB antibody (EMD Chemicals) to crosslink CTB and lipid rafts. After washing with PBS, cells were fixed in 4% PFA for 20 min at 4°C, mounted with a Prolong Antifade Kit with DAPI (Invitrogen) and images were captured with a Leica DM IRE2 fluorescent microscope.

### **Cell fractionation**

Lipid rafts (light membrane fractions) were isolated using a detergent-free, discontinuous gradient ultracentrifugation method<sup>14</sup>. Briefly, HUVEC were washed twice with ice-cold PBS and cells were scraped from the plate in 0.5 M sodium carbonate buffer (pH 11.0) containing a protease inhibitor cocktail (Sigma), homogenized and sonicated 3 × 10 sec. Samples were adjusted to 45% sucrose by adding a 90% sucrose solution in MBS (25 mM Mes, 0.15 M NaCl, pH 6.5) and placed into ultracentrifugation tubes. A 5-35% sucrose

discontinuous gradient was formed above the sample, followed by ultracentrifugation at  $35 \times 10^3$  rpm for 18 hours at 4°C in a SW-41 rotor (Beckman). Ten 1 ml fractions were collected from the top to the bottom of each gradient. The lipid rafts fraction (fraction 5) and the non-lipid rafts fraction (fraction 10) were used for further analysis, which included measurements of protein concentration and immunoblotting. Thirty  $\mu$ l of lipid rafts and non-lipid rafts fractions (adjusted to load equal protein concentrations of each sample) were run on SDS-PAGE, transferred to PVDF membranes and blotted with the indicated antibodies.

### **Caveolin-1 and VEGFR2 colocalization**

HUVEC plated on chamber coverglass (Lab-Tek™ II) were incubated for 4 hours with 0.1  $\mu$ g/ml hAIBP, 50  $\mu$ g/ml HDL<sub>3</sub> or 0.1  $\mu$ g/ml hAIBP + 50  $\mu$ g/ml HDL<sub>3</sub>, and the cells were washed with PBS and fixed with warm 4% PFA for 15min at room temperature. HUVEC were permeabilized, blocked, and incubated with anti-Caveolin-1 (BD Biosciences) and anti-VEGFR2 (Cell Signaling Technology) antibodies, followed by incubation with anti-mouse IgG-Alexa Fluor 488 and anti-rabbit IgG-Cy3 antibodies. Images were captured using a Nikon Eclipse Ti inverted fluorescent microscope operating in TIRF mode. Raw TIFF images of Caveolin-1 and VEGFR2 were analyzed using JACoP algorithm<sup>31</sup> in Image J. Colocalization was quantified using Pearson's coefficient.

### **VEGFR2 endocytosis**

HUVEC were incubated for 4 hours with 0.1  $\mu$ g/ml hAIBP, 50  $\mu$ g/ml HDL<sub>3</sub> or 0.1  $\mu$ g/ml hAIBP + 50  $\mu$ g/ml HDL<sub>3</sub>, followed by a 20 min incubation with 50 ng/ml VEGF. Cells were fixed and stained with antibodies against VEGFR2 and the early endosomal marker EEA-1-FITC (BD Biosciences). Images were captured with a Nikon Eclipse Ti inverted fluorescent microscope. VEGFR2 and EEA-1 colocalization was quantified using Pearson's coefficient with the JACoP plugin loaded to ImageJ<sup>31</sup>.

### **VEGFR2 dimerization assay**

The assay was carried out as described in reference<sup>32</sup>. Two days after plating  $1 \times 10^6$  HUVEC in a 10 cm dish, the cells were starved overnight in 0.5% FBS-EBM. Next day, cells were incubated with hAIBP and/or HDL<sub>3</sub>, followed by a 20 min incubation with 50 ng/ml VEGF and then crosslinked with 1 mg/ml bis-sulfosuccinimidyl (Thermo Scientific) for 30 min on ice. Cell lysates were immunoprecipitated with an anti-VEGFR2 antibody immobilized on agarose beads. The beads were washed and the eluted samples were run on SDS-PAGE, followed by immunoblotting with the VEGFR2 antibody.

### **HUVEC migration assay**

Serum starved HUVEC were pretreated with 50  $\mu$ g/ml HDL<sub>3</sub>, 0.2  $\mu$ g/ml hAIBP, or 50  $\mu$ g/ml HDL<sub>3</sub> + 0.2  $\mu$ g/ml hAIBP for 4 hours at 37°C in 5% LPDS/EBM, harvested from the plate, washed, resuspended in 5% LPDS/EBM and added to the transwell (8  $\mu$ m pore size). VEGF was added to the lower chamber at 20 ng/ml. Following a 4 hour incubation, the transwell membranes were fixed in ice-cold methanol for 10 min and stained with filtered 0.5% Crystal Violet for 10 min, and transmigrated cells were counted.

## Zebrafish

Wild type AB and transgenic *Tg(fli1:egfp)<sup>y1</sup>* and *Tg(flk1:ras-cherry)<sup>s896</sup>* zebrafish lines<sup>19,33</sup> were kindly provided by Dr. David Traver and Neil Chi (UCSD). Zebrafish were maintained as previously described<sup>34</sup>, and all experimental procedures were approved by the UCSD IACUC.

## Confocal microscopy

Confocal imaging was carried out as previously described<sup>35</sup>. Briefly, anaesthetized zebrafish embryos (treated at 24 hpf with 0.003% PTU) were housed in a sealed chamber (Invitrogen) in a small drop of 0.02% tricaine (Sigma) containing E3 medium and imaged using a Nikon C1-si confocal microscope. Z-stacks were acquired with a 1-3  $\mu\text{m}$  step, and images were 3D rendered and analyzed using Imaris® software (Bitplane). All 3D reconstructions were performed with the same threshold settings.

## Morpholino oligonucleotide injections

To knock down gene expression, 4-8 ng of morpholino antisense oligonucleotides (MO; synthesized by GeneTools) were injected into one-cell stage embryos. A control MO was derived from the *zaibp2* sequence, with 5 mismatched oligonucleotides.

Control MO: TGAGCTTCATGTTCATTTATTCCGC; *zaibp2* MO (*zaibp2* MO1): TGTGGTTCATCTTGATTTATTCCGC; *zaibp2* splicing MO (*zaibp2* MO2):TGTTGAGTGTCAGACAAACCTTGGT *zaibp1* MO: TCTGTATTCAAATCAGACGCTCAGT; *abca1* MO: AACCCAACTGAGTGGAGACAGCCAT; *abcg1* MO: AAAAGGCTGCCATGAGACATGCCAT.

## Quantitative analysis of cell sprouts in segmental arteries (SeA) and subintestinal veins (SIV)

To determine changes in segmental artery cell sprouts in embryos injected with MO targeting *zaibp2*, *zaibp1*, *abca1* and/or *abcg1*, we counted abnormal projections in 4 to 6 pairs of segmental arteries in adjacent somite boundaries in each zebrafish. For each set of injections, 15 embryos (i.e. 60-90 sprouts) were examined. Values were expressed as a number of ectopic sprouts per SeA. To examine sprouts in SIV, only the sprouts moving in the ventral direction out of the SIV were counted. Values were expressed as a number of ventral SIV sprouts per zebrafish.

## Measuring membrane lipid order with polarity-sensitive probe

The experiments were carried out as described in references<sup>36,37</sup>. Briefly, live *Tg(flk1:ras-cherry)<sup>s896</sup>* zebrafish embryos were incubated with 5  $\mu\text{M}$  Laurdan (Invitrogen) at 28°C for 30 min. The concentration of a Laurdan stock solution was measured using OD at 365 nm and an extinction coefficient of 19000  $\text{cm}^{-1}\text{M}^{-1}$ . After incubation with Laurdan, embryos were incubated with E3 medium for additional 30 min, fixed in PFA for 4 hours at room temperature, deyolked, and embedded in 1% low melting temperature agarose for imaging. Images were captured with a Leica SP5 confocal/multiphoton system, using a water

immersion 20× objective. The confocal mode was used to capture mCherry fluorescence and the multiphoton mode was used to capture Laurdan images (ex 800 nm, em 400-460 nm and 470-530 nm) in the same embryos. The multiphoton results were displayed as pseudocolored GP (a measure of the membrane lipid order) images, derived from Laurdan ratiometric measurements and using a ImageJ plug-in as described<sup>36</sup>. The quantitative data were obtained by measuring GP values in the areas corresponding to tip cells (top 1/3 of the SeA length), stalk cells (bottom 2/3 of the SeA length) and the dorsal aorta in several individual, mCherry-masked z-sections. This method ensured that GP values were derived only from EC (e.g. from the areas where mCherry was in focus in each z-section). The GP images in Fig. 3d were composed each from four to five individual z-sections, with a minimal overlap of mCherry-masked GP images.

### Whole mount in situ hybridization

WISH was carried out as described<sup>38-40</sup>. Briefly, wild type embryos or morphants at indicated developmental stages were fixed with 4% PFA and the embryos older than 24 hpf were permeabilized with 10 µg/ml proteinase K (Roche). Subsequently, the embryos were pre-hybridized at 70°C for 4-6 hours, and then hybridized with a digoxigenin-labeled *zaihp2* antisense probe at 65°C for 2 days. Both the control sense and anti-sense RNA probes were directly synthesized from *zaihp2* full length gene using a Roche T7/SP6 RNA or Ambion T3 RNA synthesis kit. After extensive wash, hybridized RNA was detected by immunohistochemistry using an alkaline phosphatase-conjugated antibody against digoxigenin (Roche) and a chromogenic substrate nitro blue tetrazolium (NBT) (Sigma) and 5-bromo-4-chloro-3-indolyl phosphate (BCIP)<sup>38</sup> (Sigma). A similar procedure was performed with *tie2*, *vegfr2*, *vegfr3*, *fli1* and *cdh5* probes. Double WISH was performed as described<sup>41</sup>. Both digoxigenin-labeled *zaihp2* and fluorescein-labeled *myod* were hybridized with the same embryos. The embryos were then first incubated with alkaline phosphatase-conjugated anti-fluorescein Ab, and fast red (Roche) was used as a substrate. Subsequently, the embryos were washed, fixed with 4% PFA and incubated with anti-digoxigenin Ab conjugated alkaline phosphatase, and then NBT/BCIP was used as a chromogenic substrate.

### Transplantation experiments

Cell transplantation was performed as described<sup>39</sup>, with different combinations of donors and recipients as indicated in Fig. 4a. Donor embryos were of the *Tg(fli1:egfp)<sup>y1</sup>* origin, and recipient embryos were of the wild type origin. At the one-cell stage, donor *Tg(fli1:egfp)<sup>y1</sup>* embryos were injected with rhodamine-labeled dextran (Mini-Ruby, Invitrogen) as a lineage tracer. At the sphere stage (approximately 4 hpf), embryos were dechorionated by 0.4 mg/ml pronase (Sigma) and transferred to agarose wells (Adaptive Science Tools, Worcester, MA). Approximately 20-40 cells from the margin of a donor embryo were transferred to the margin of a recipient embryo. The recipient embryos were subsequently grown at 28°C and imaged at 72 hpf. Endothelial cells in chimeric zebrafish originating from donor embryos were visualized by their green fluorescence using a Leica M165FC fluorescent stereoscope. For detailed analysis, images were captured using a Nikon C1-si confocal microscope. Numbers of ectopic branches in each fluorescent SeA were counted.

### Real time PCR

Real time PCR was performed using a Rotor Gene Q qPCR machine (Qiagen). Real time PCR master mix Platinum SYBR Green qPCR SuperMix was from Invitrogen. The primers were synthesized by IDT. The PCR program was: 50°C for 2 minutes (UDG incubation), 95°C for 2 minutes, 40 cycles of: 95°C for 15 seconds, 60°C for 1 minute. Primer sequences: *fli1* (F): CTTGGCACGTTGCCTTGATAAG, *fli1* (R): CCTTCATATCTGAGAGTGATCCC; *tie2* (F): GCGATGGATGGCAATAGAGT, *tie2* (R): CGACAGCAGGATCTGAGAGA; *vegfr2* (F): TCCACGAGGGTGGGCAGTCA; *vegfr2* (R): AGACGGGTGGTGTGGAGTAACGA. *kdrb* (F): TGCCACATGGAGCTGCTAGCA; *kdrb* (R): TGTGGCACATTCAACCACATGAGC. *β-actin* (F): CTCTTCCAGCCTTCCTCCT, *β-actin* (R): GGTGGTTCGTTGTTGAAT.

### Immunoblot of zebrafish lysates

Zebrafish were lysed on ice with a lysis buffer (50 mM Tris-HCl, pH 7.5, 4 mM sodium deoxycholate, 1% Triton X 100, 150 mM NaCl, 1 mM EDTA, and a protease inhibitor cocktail from Sigma). Protein content was determined with a DC protein assay kit (BioRad) and equal protein amounts of the cell lysates were run on a 4-12% Bis-Tris SDS-PAGE with MOPS buffer (Invitrogen) and then transferred to a PVDF membrane (Invitrogen). The blots were probed with appropriate antibodies against specific phosphorylated and non-phosphorylated proteins (Cell Signaling Technology), secondary antibodies conjugated with HRP and developed using a Super Signal West Dura substrate (Pierce).

### Filipin staining

Filipin staining of embryos was performed as described<sup>42</sup>. Zebrafish were fixed with 4% PFA overnight at 4°C. The fixed fish were incubated overnight with 0.05% filipin (Sigma) in PBS with 1% sheep serum, and then washed 3 times with PBS. Images were captured immediately with a Leica M165FC fluorescent stereoscope and quantified.

### Total lipid extraction and free cholesterol measurements in zebrafish

Total lipid was extracted from zebrafish embryos as we previously described<sup>28</sup>. In brief, trunk/tail segments were dissected from fifty 24 hpf embryos and pooled together. The tissue was homogenized and supplemented with 50 µg stigmasterol, an internal standard to control for recovery of extracted sterols. Total lipid extraction was performed with 1:2 methanol/dichloromethane. No saponification of cholesterol esters was performed because the goal of this study was to measure free cholesterol, the form of cholesterol transferred from the cells via ABC transporters to ApoA-I/HDL. Cholesterol and stigmasterol were measured with a Shimadzu GC-2014 gas chromatograph using a 30 m × 0.25 mm (i.d.) ZB-5HT inferno capillary column, film thickness 0.2 µm (Phenomenex). Cholesterol levels were normalized to protein and then to the levels in embryos injected with control MO.

### Supplementary Material

Refer to Web version on PubMed Central for supplementary material.

## Acknowledgments

We thank David Traver, Neil Chi, Joseph Witztum, Richard Klemke, Deborah Yelon, Tracy Handel, Konstantin Stoletov, Wilson Clements, Claire Pouget, Zayra Garavito-Aguilar, Ararat Ablooglu, Ruiling Zhang, Xiaohong Yang, Mila Angert, Kersi Pestonjamas and Jennifer Santini (UC San Diego), Catherine Hedrick, Klaus Ley, Duygu Sag, Prithu Sundd and Amy Wu (La Jolla Institute for Allergy and Immunology), Sean Trzaska (New York University), Shao Jun Du (University of Maryland), Bettina Schmid and Christian Haass (Ludwig-Maximilians-University München, Germany), Dylan Owen and Astrid Magenau (University of New South Wales, Australia), Arndt Siekmann (Max-Planck Institute for Molecular Biomedicine), and Christoph Binder (Medical University of Vienna, Austria) for many helpful discussions, technical assistance and/or for providing reagents and access to equipment for this study. The project was supported by the NIH grants HL093767 (Y.I.M.), HL055798 (Y.I.M.) and HL114734 (L.F.), and the fellowship 18FT-0137 from the UC Tobacco-Related Disease Program (L.F.), as well as the UCSD Neuroscience Microscopy Facility Grant P30 NS047101.

## References

1. Bodzioch M, et al. The gene encoding ATP-binding cassette transporter 1 is mutated in Tangier disease. *Nat Genet.* 1999; 22:347–351. [PubMed: 10431237]
2. Rust S, et al. Tangier disease is caused by mutations in the gene encoding ATP-binding cassette transporter 1. *Nat Genet.* 1999; 22:352–355. [PubMed: 10431238]
3. Klucken J, et al. ABCG1 (ABC8), the human homolog of the *Drosophila* white gene, is a regulator of macrophage cholesterol and phospholipid transport. *Proc Natl Acad Sci USA.* 2000; 97:817–822. [PubMed: 10639163]
4. Yvan-Charvet L, et al. ATP-Binding Cassette Transporters and HDL Suppress Hematopoietic Stem Cell Proliferation. *Science.* 2010; 328:1689–1693. [PubMed: 20488992]
5. Armstrong AJ, Gebre AK, Parks JS, Hedrick CC. ATP-binding cassette transporter G1 negatively regulates thymocyte and peripheral lymphocyte proliferation. *J Immunol.* 2010; 184:173–183. [PubMed: 19949102]
6. Bensinger SJ, et al. LXR signaling couples sterol metabolism to proliferation in the acquired immune response. *Cell.* 2008; 134:97–111. [PubMed: 18614014]
7. Ritter M, et al. Cloning and Characterization of a Novel Apolipoprotein A-I Binding Protein, AI-BP, Secreted by Cells of the Kidney Proximal Tubules in Response to HDL or ApoA-I. *Genomics.* 2002; 79:693–702. [PubMed: 11991719]
8. Jha KN, et al. Biochemical and Structural Characterization of Apolipoprotein A-I Binding Protein, a Novel Phosphoprotein with a Potential Role in Sperm Capacitation. *Endocrinology.* 2008; 149:2108–2120. [PubMed: 18202122]
9. Stefulj J, et al. Human Endothelial Cells of the Placental Barrier Efficiently Deliver Cholesterol to the Fetal Circulation via ABCA1 and ABCG1. *Circ Res.* 2009; 104:600–608. [PubMed: 19168441]
10. Terasaka N, et al. ABCG1 and HDL protect against endothelial dysfunction in mice fed a high-cholesterol diet. *J Clin Invest.* 2008; 118:3701–3713. [PubMed: 18924609]
11. Fessler MB, Parks JS. Intracellular lipid flux and membrane microdomains as organizing principles in inflammatory cell signaling. *J Immunol.* 2011; 187:1529–1535. [PubMed: 21810617]
12. Mendez AJ, et al. Membrane Lipid Domains Distinct from Cholesterol/Sphingomyelin-Rich Rafts Are Involved in the ABCA1-mediated Lipid Secretory Pathway. *J Biol Chem.* 2001; 276:3158–3166. [PubMed: 11073951]
13. Murphy AJ, et al. High-Density Lipoprotein Reduces the Human Monocyte Inflammatory Response. *Arterioscler Thromb Vasc Biol.* 2008; 28:2071–2077. [PubMed: 18617650]
14. Noghero A, et al. Liver X Receptor Activation Reduces Angiogenesis by Impairing Lipid Raft Localization and Signaling of Vascular Endothelial Growth Factor Receptor-2. *Arterioscler Thromb Vasc Biol.* 2012; 32:2280–2288. [PubMed: 22723445]
15. Oshikawa J, et al. Novel role of p66Shc in ROS-dependent VEGF signaling and angiogenesis in endothelial cells. *Am J Physiol Heart Circ Physiol.* 2012; 302:H724–H732. [PubMed: 22101521]
16. Ikeda S, et al. Novel Role of ARF6 in Vascular Endothelial Growth Factor-Induced Signaling and Angiogenesis. *Circ Res.* 2005; 96:467–475. [PubMed: 15692085]

17. Liao, Wx, et al. Compartmentalizing VEGF-Induced ERK2/1 Signaling in Placental Artery Endothelial Cell Caveolae: A Paradoxical Role of Caveolin-1 in Placental Angiogenesis in Vitro. *Mol Endocrinol.* 2009; 23:1428–1444. [PubMed: 19477952]
18. Eichmann A, Simons M. VEGF signaling inside vascular endothelial cells and beyond. *Curr Opin Cell Biol.* 2012; 24:188–193. [PubMed: 22366328]
19. Lawson ND, Weinstein BM. In Vivo Imaging of Embryonic Vascular Development Using Transgenic Zebrafish. *Dev Biol.* 2002; 248:307–318. [PubMed: 12167406]
20. Torres-Vazquez J, et al. Semaphorin-plexin signaling guides patterning of the developing vasculature. *Dev Cell.* 2004; 7:117–123. [PubMed: 15239959]
21. Dean M, Annilo T. Evolution of the ATP-binding cassette (ABC) transporter superfamily in vertebrates. *Ann Rev Genomics Hum Genet.* 2005; 6:123–142. [PubMed: 16124856]
22. Archer A, et al. Transcriptional activity and developmental expression of liver X receptor (lxr) in Zebrafish. *Dev Dyn.* 2008; 237:1090–1098. [PubMed: 18297735]
23. Whetzel AM, et al. ABCG1 Deficiency in Mice Promotes Endothelial Activation and Monocyte-Endothelial Interactions. *Arterioscler Thromb Vasc Biol.* 2010; 30:809–817. [PubMed: 20110576]
24. Avraham-Davidi I, et al. ApoB-containing lipoproteins regulate angiogenesis by modulating expression of VEGF receptor 1. *Nat Med.* 2012; 18:967–973. [PubMed: 22581286]
25. Carmona G, et al. Role of the small GTPase Rap1 for integrin activity regulation in endothelial cells and angiogenesis. *Blood.* 2009; 113:488–497. [PubMed: 18805968]
26. Catanzariti AM, Soboleva TA, Jans DA, Board PG, Baker RT. An efficient system for high-level expression and easy purification of authentic recombinant proteins. *Protein Sci.* 2004; 13:1331–1339. [PubMed: 15096636]
27. O'Connell BJ. Cellular Physiology of Cholesterol Efflux in Vascular Endothelial Cells. *Circulation.* 2004; 110:2881–2888. [PubMed: 15492319]
28. Fang L, et al. Oxidized cholesteryl esters and phospholipids in zebrafish larvae fed a high cholesterol diet: macrophage binding and activation. *J Biol Chem.* 2010; 285:32343–32351. [PubMed: 20710028]
29. Gao F, et al. L-5F, an apolipoprotein A-I mimetic, inhibits tumor angiogenesis by suppressing VEGF/basic FGF signaling pathways. *Integr Biol (Camb).* 2011; 3:479–489. [PubMed: 21283904]
30. Bellacen K, Lewis EC. Aortic ring assay. *J Vis Exp.* 2009
31. Bolte S, Cordeliers FP. A guided tour into subcellular colocalization analysis in light microscopy. *J Microsc.* 2006; 224:213–232. [PubMed: 17210054]
32. Chung TW, et al. Ganglioside GM3 inhibits VEGF/VEGFR-2-mediated angiogenesis: direct interaction of GM3 with VEGFR-2. *Glycobiology.* 2009; 19:229–239. [PubMed: 18974200]
33. Chi NC, et al. Foxn4 directly regulates tbx2b expression and atrioventricular canal formation. *Genes Dev.* 2008; 22:734–739. [PubMed: 18347092]
34. Westerfield, M. *The Zebrafish Book.* (University of Oregon Press; Eugene, Oregon: 2007.
35. Stoletov K, et al. Vascular lipid accumulation, lipoprotein oxidation, and macrophage lipid uptake in hypercholesterolemic zebrafish. *Circ Res.* 2009; 104:952–960. [PubMed: 19265037]
36. Owen DM, Rentero C, Magenau A, Abu-Siniyeh A, Gaus K. Quantitative imaging of membrane lipid order in cells and organisms. *Nat protocols.* 2012; 7:24–35. [PubMed: 22157973]
37. Gaus K, Le Lay S, Balasubramanian N, Schwartz MA. Integrin-mediated adhesion regulates membrane order. *J Cell Biol.* 2006; 174:725–734. [PubMed: 16943184]
38. Thisse C, Thisse B. High-resolution in situ hybridization to whole-mount zebrafish embryos. *Nat Protoc.* 2008; 3:59–69. [PubMed: 18193022]
39. Siekmann AF, Lawson ND. Notch signalling limits angiogenic cell behaviour in developing zebrafish arteries. *Nature.* 2007; 445:781–784. [PubMed: 17259972]
40. Lawson ND, et al. Notch signaling is required for arterial-venous differentiation during embryonic vascular development. *Development.* 2001; 128:3675–3683. [PubMed: 11585794]
41. Jowett T. Analysis of protein and gene expression. *Methods Cell Biol.* 1999; 59:63–85. [PubMed: 9891356]

42. Schwend T, Loucks EJ, Snyder D, Ahlgren SC. Requirement of Npc1 and availability of cholesterol for early embryonic cell movements in zebrafish. *J Lipid Res.* 2011; 52:1328–1344. [PubMed: 21576600]

Author Manuscript

Author Manuscript

Author Manuscript

Author Manuscript

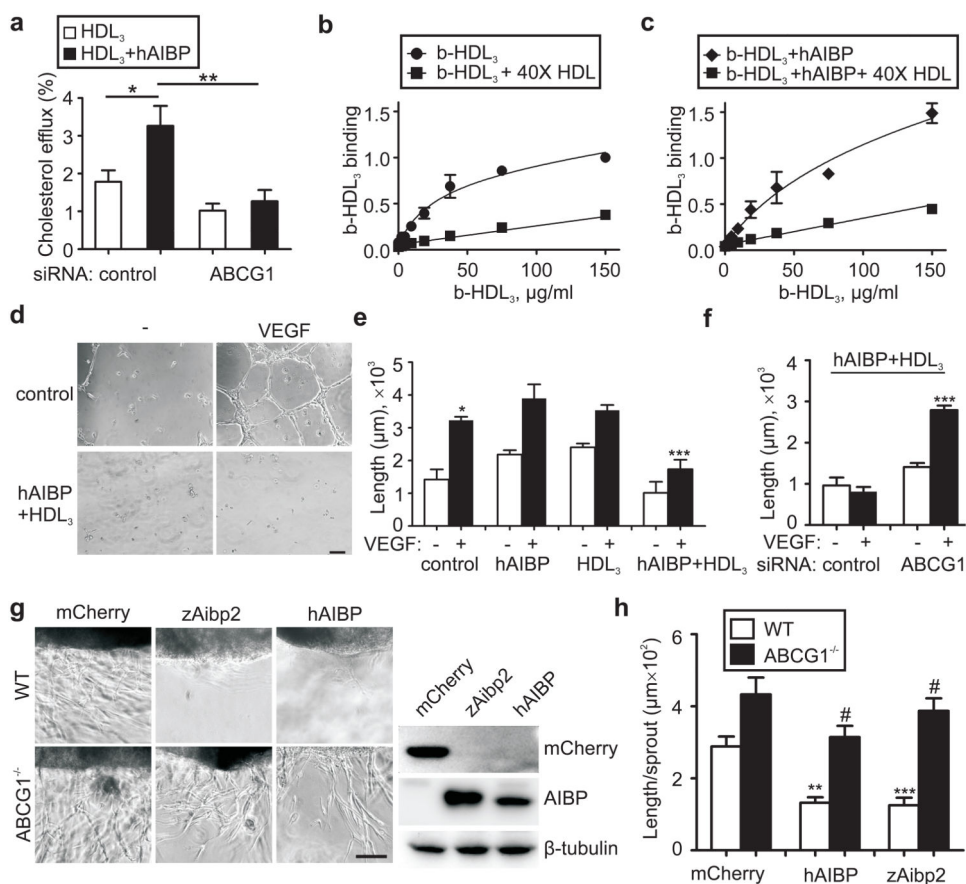


**Figure 1. Role of AIBP in cholesterol efflux from EC and *in vitro* angiogenesis**

**a**, hAIBP mediated-cholesterol efflux and effect of ABCG1 knockdown. HUVEC were transfected with control or ABCG1 siRNA, preloaded with  $^3\text{H}$ -cholesterol and incubated for 1 hour with 50  $\mu\text{g}/\text{ml}$  HDL<sub>3</sub> in the presence or absence of 0.2  $\mu\text{g}/\text{ml}$  hAIBP. Efflux was measured as the  $^3\text{H}$  counts in the medium divided by the sum of  $^3\text{H}$  counts in the medium and the cells. Mean $\pm$ SE; n=6. **b** and **c**, Effect of hAIBP on HDL<sub>3</sub> binding to HUVEC. HUVEC were incubated on ice with the indicated concentration of biotinylated HDL<sub>3</sub> (b-HDL<sub>3</sub>), in the presence or absence of hAIBP (at a 0.1:50 w/w hAIBP:HDL<sub>3</sub> ratio) and 40 $\times$  excess of unlabeled HDL. Each data point is Mean $\pm$ SE from 3 to 7 independent experiments. The binding parameters for b-HDL<sub>3</sub>/HUVEC binding were calculated as  $B_{\text{max}} = 0.8 \pm 0.1$  and  $K_d = (0.33 \pm 0.10) \times 10^{-6}$  M in absence of hAIBP (panel **b**;  $R^2=0.92$ ,  $Sy.x=0.1$ ), and  $B_{\text{max}}=1.5 \pm 0.4$  and  $K_d=(1.03 \pm 0.10) \times 10^{-6}$  M in the presence of hAIBP (panel **c**;  $R^2=0.94$ ,  $Sy.x=0.1$ ). The differences in  $B_{\text{max}}$  and  $K_d$  values were statistically significant ( $p<0.01$  and  $p<0.05$ , respectively). **d**, Effect of hAIBP and HDL<sub>3</sub> on EC tube formation. HUVEC were preincubated with or without 50  $\mu\text{g}/\text{ml}$  HDL<sub>3</sub> + 0.1  $\mu\text{g}/\text{ml}$  hAIBP for 4 hours. Cells were then seeded on Matrigel, in the presence or absence of 20 ng/ml VEGF, and imaged following a 12-hour incubation. Scale, 100  $\mu\text{m}$ . **e**, The length of EC tubes in the experiment illustrated in 1d and Supplementary Fig. 4. Mean $\pm$ SE; n=5. **f**, Requirement for ABCG1 in hAIBP inhibition of angiogenesis. HUVEC were transfected with control or ABCG1 siRNA and assayed as in 1d. Mean $\pm$ SE; n=6. **g**, Mouse aortic ring angiogenesis assay. Aortic rings from C57BL6 and *Abcg1*<sup>-/-</sup> mice were embedded in Matrigel. HEK293

cells transiently expressing mCherry, zAibp2 or hAIBP were inserted approximately 0.5 mm away from the aortic ring, and the plates were incubated with 10 ng/ml VEGF for 7 days. Images show the edge of the aortic rings facing the HEK293 cell clusters. Immunoblots show expression of hAIBP and zAibp2 (both detected with a Flag tag antibody) and mCherry in HEK293 cells. **h**, The length of aortic ring sprouts. Mean±SE; n=10. In all panels: #, not significant; \*, p<0.05; \*\*, p<0.01; \*\*\*, p<0.001.

Author Manuscript

Author Manuscript

Author Manuscript

Author Manuscript

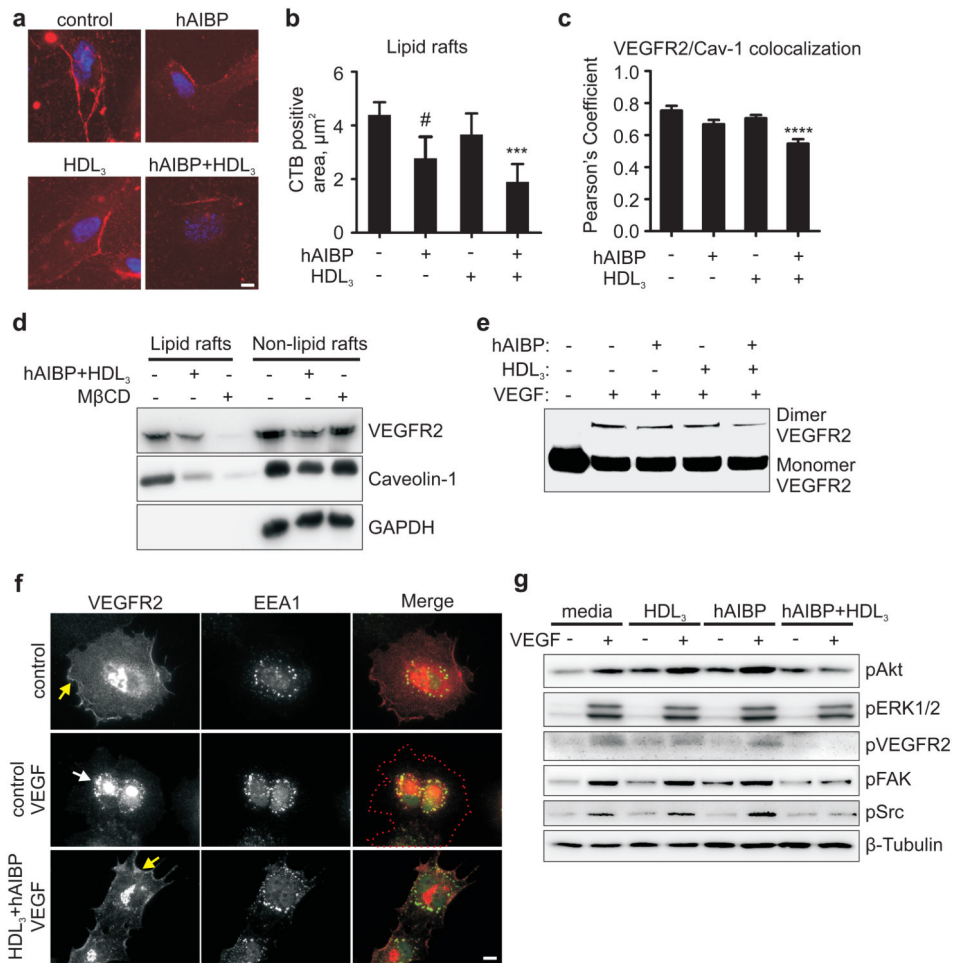


**Figure 2. Effect of AIBP on HUVEC lipid rafts, VEGFR2 localization, dimerization and signaling**

**a**, Effect of hAIBP and HDL<sub>3</sub> on lipid rafts. HUVEC were preincubated with 50  $\mu\text{g}/\text{ml}$  HDL<sub>3</sub>, 0.1  $\mu\text{g}/\text{ml}$  hAIBP, or 50  $\mu\text{g}/\text{ml}$  HDL<sub>3</sub> + 0.1  $\mu\text{g}/\text{ml}$  hAIBP for 4 hours. Cells were stained for nuclei (blue, DAPI) and for lipid rafts (red, cholera toxin B (CTB) + anti-CTB antibody). Scale, 10  $\mu\text{m}$ . **b**, The area of lipid rafts per cell. Mean $\pm$ SE; n=10; \*\*, p<0.01; #, p=0.08. **c**, Effect of hAIBP and HDL<sub>3</sub> on caveolin-1 and VEGFR2 surface localization. HUVEC were incubated with hAIBP and/or HDL<sub>3</sub> as in 2a, fixed and stained with antibodies to caveolin-1 and VEGFR2. Images were captured using TIRF microscopy (Supplementary Fig. 6) and Pearson's coefficient was calculated to assess surface colocalization of VEGFR2 with caveolin-1. Mean $\pm$ SE; n=38-50; \*\*\*\*, p<0.001. **d**, VEGFR2 and caveolin-1 localization to lipid rafts. HUVEC were incubated with 20  $\mu\text{g}/\text{ml}$  cholesterol-M $\beta$ CD for six hours, followed by a 1 hour incubation with or without 50  $\mu\text{g}/\text{ml}$  HDL<sub>3</sub> + 0.1  $\mu\text{g}/\text{ml}$  hAIBP, or a 30 min incubation with 10 mM M $\beta$ CD. HUVEC lysates were separated into lipid rafts and non-lipid rafts fractions by ultracentrifugation, run on SDS-PAGE and blotted with VEGFR2 and caveolin-1 antibodies. **e**, Effect of hAIBP and HDL<sub>3</sub> on VEGFR2 dimerization. HUVEC were preincubated with HDL<sub>3</sub> and/or hAIBP as in 1a, followed by a 20 min stimulation with 50 ng/ml VEGF. Cells were treated with a crosslinking reagent, lysed and immunoprecipitated with a VEGFR2 antibody. Monomers and crosslinked dimers

of VEGFR2 were visualized on western blot. **f**, Effect of hAIBP and HDL<sub>3</sub> on VEGFR2 endocytosis. HUVEC were preincubated with or without 50 µg/ml HDL<sub>3</sub> + 0.1 µg/ml hAIBP for 4 hours, then stimulated with 50 ng/ml VEGF for 20 min, fixed and stained with antibodies to VEGFR2 (red) and the early endosome marker EEA-1 (green). Yellow and white arrows point to the surface and endosomal localization of VEGFR2. Red dotted line traces cell contour. Scale, 10µm. **g**, Effect of hAIBP and HDL<sub>3</sub> on VEGFR2 signaling. HUVEC were preincubated with HDL<sub>3</sub> and/or hAIBP as in 2a, followed by a 20 min stimulation with 50 ng/ml VEGF. Total cell lysates were run on SDS-PAGE and probed as indicated.

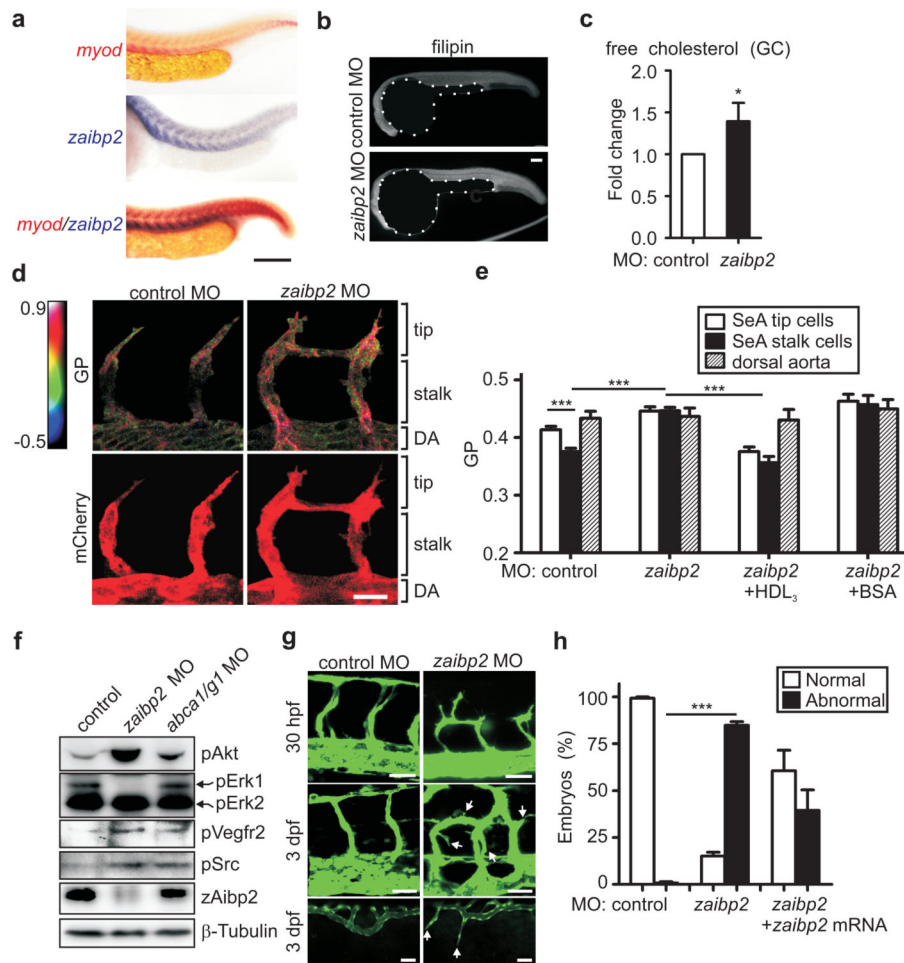


**Figure 3. Effect of Aibp deficiency on zebrafish cholesterol, membrane lipid order, Vegfr2 signaling and angiogenesis**

**a**, Tissue distribution of *zaibp2* mRNA in zebrafish embryos. Embryos at 24 hpf were fixed and WISH was performed with antisense *myod* and *zaibp2* probes. Scale, 100  $\mu$ m. **b-c**, Free cholesterol levels in *zaibp2* morphants. **b**, Zebrafish embryos were injected with 8 ng of either control MO or *zaibp2* MO. Twenty four hpf control and *zaibp2* morphants were stained with filipin to detect free cholesterol in embryos. Note the yolks are artificially masked on the images. **c**, At 24 hpf, the trunk area (without yolk) was dissected, total lipids extracted, and free cholesterol levels determined by gas chromatography (GC). The cholesterol levels were normalized to the protein content and then to the values in control MO embryos. 50-70 embryos were pooled for each sample. Mean $\pm$ SE; n=4; \*, p<0.05. **d**, Effect of *zaibp2* MO on SeA membrane lipid order. *Tg(flkl:ras-cherry)*<sup>s896</sup> embryos were injected with control or *zaibp2* MO as in 3b and at 24 hpf were stained with 5  $\mu$ M Laurdan. In the same embryos, confocal images of mCherry fluorescence (bottom images) and the multiphoton images of Laurdan fluorescence (ex 800 nm, em 400-460 nm and 470-530 nm) were captured. The multiphoton results (top row images) are displayed as pseudocolored GP (generalized polarization, a measure of the membrane lipid order) images, cropped to show only the vasculature, i.e. mCherry-positive areas. Scale, 20  $\mu$ m. **e**, The graph shows GP values in the areas corresponding to tip and stalk cells of growing SeA and the dorsal aorta

(DA) as indicated in 3d. Some one-cell stage embryos were coinjected with 1 nl of 10 mg/ml human HDL<sub>3</sub> or BSA. Note the Y-scale is from 0.2 to 0.5. Mean±SE; n=44-119 SeA in 25-49 embryos; \*\*\*, p<0.001. **f**, Phosphorylation of signaling proteins. Lysates of 24 hpf control (8 ng control MO), *zaibp2* (8 ng *zaibp2* MO) and *abca1/g1* (4 ng *abca1* MO + 4ng *abcg1* MO) morphants were separated on SDS-PAGE and immunoblotted as indicated. **g**, Angiogenic defects in *zaibp2* morphants. One-cell stage *Tg(fli1:egfp)<sup>y1</sup>* zebrafish embryos were injected with 8 ng of either control or *zaibp2* MO. The images are of SeA in 30 hpf embryos (top row), and SeA (middle row) and of SIV (bottom row) in 3 dpf embryos. Arrows point to dysregulated sprouts. Scale, 25 μm. **h**, Quantification of the number of embryos with normal and abnormal angiogenesis (SeA with ectopic branching). The abnormal angiogenesis was partially rescued by coinjection of 40 pg of *zaibp2* mRNA lacking the MO targeting site. Mean±SE; n=100-149. \*\*\*, p<0.001.

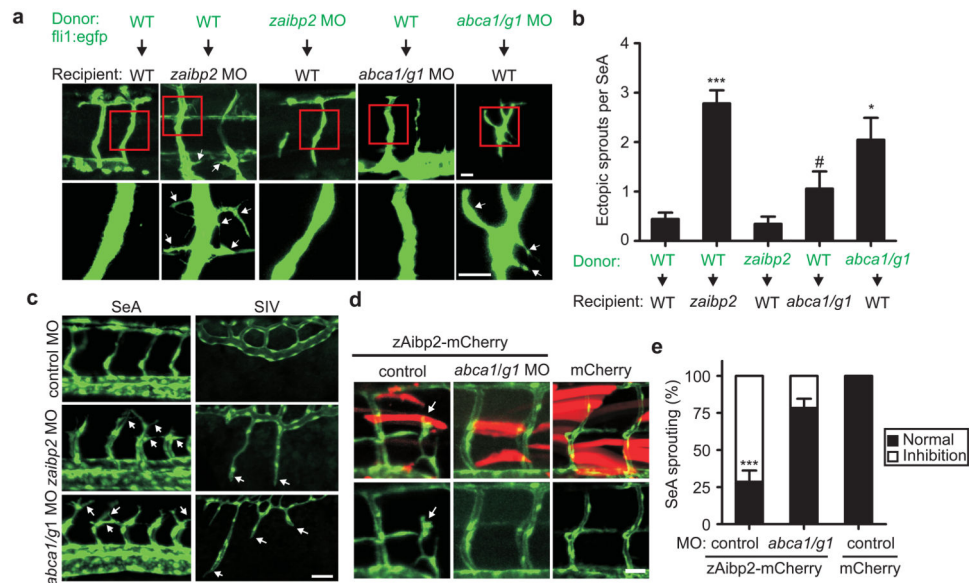


**Figure 4. Effect of Aibp and Abca1/Abcg1 deficiency on zebrafish angiogenesis**

**a**, Mosaic expression analysis of EC branching in control, *zaibp2* and *abca1/abcg1* knockdown embryos. At 4 hpf, cells were isolated from donor embryos and transplanted into recipient embryos. Recipient embryos were analyzed at 3 dpf. Arrows point to aberrant ectopic branches/sprouts. Scale, 25  $\mu$ m. **b**, Numbers of ectopic branches/filopodial projections per SeA. Mean $\pm$ SE; n=8-16. #, not significant; \*, p<0.05; \*\*\*, p<0.001. **c**, Angiogenic defects in *abca1/abcg1* morphants. One-cell stage embryos were injected with 8 ng of control MO, 8 ng *zaibp2* MO, or 4 ng *abca1* MO + 4 ng *abcg1* MO. Images of SeA (30 hpf) and SIV (3 dpf) are shown. Scale, 50  $\mu$ m. **d**, Knockdown of *abca1/g1* cancels the effect of zAibp2 overexpression. One-cell stage embryos were injected with 2 nl of 100 ng/ $\mu$ l *myog:zaibp2-mCherry*, *myog:zaibp2-mCherry* + *abca1/g1* MO, or *myog:mCherry*. The arrow points to an aberrant SeA at the site of zAibp2-mCherry expression. Scale, 20 $\mu$ m. **e**, Abnormal SeA formation was quantified in 8-16 embryos per group. Mean $\pm$ SE; \*\*\* p<0.001.